Sandwich-Like, Stacked Ultrathin Titanate Nanosheets for Ultrafast Lithium Storage

Jiehua Liu, Jun Song Chen, Xiangfeng Wei, Xiong Wen Lou, and Xue-Wei Liu**

Nanomaterials in architecture for green energy conversion and/or storage provide one of the most desirable approaches to alleviate environmental and energy issues.[1–4] As a result, there is increasing interest in developing high-power anode materials, which can match with the state-of-the-art high-power cathode materials, for next generation high-performance rechargeable Li-ion batteries.[5–7] Titanium dioxide is regarded as one of the ideal candidates for high-rate anode materials, owing not only to its structural characteristics and special surface activity,[8–11] but also to its low cost, safety, and environmental benignity. The lack of open channels in bulk TiO_2 is the main drawback that restricts its capacity and rate capability for reversible lithium insertion and extraction. A reduction in the effective size and construction of open channels in the material are the main strategies currently employed to increase the rate performance.[1,4] The capacity could also be improved by reducing the path length of lithium ion migration and improving electron transport at the surface or in the bulk of the material.[10,12,13] With these strategies, the capacity of ultrafine TiO_2 nanocrystals and nanotubes, for example, is significantly enhanced at lower rates. However, their capacity and cycle life deteriorate dramatically at higher rates.[9,14–17] In this respect, significant efforts have recently been made on the fabrication of anatase TiO_2 nanosheets with exposed highly reactive (001) facets.[18–21] These TiO_2 nanosheets are shown to be an excellent host structure for lithium insertion and extraction due to the presence of exposed (001) facets and short path along the [001] direction for lithium ion diffusion.

Although the anatase framework undergoes insignificant structural distortion during lithium insertion and extraction,[22] the rate of lithium diffusion is still limited by the narrow space of the host Ti–O lattice. Also, strongly caustic NaOH and corrosive HCl or HF are commonly used for the synthesis of TiO_2 nanomaterials.[17,18] Beyond these, there is still potential danger in the high-temperature and high-pressure process in low boiling point inflammable solvents.[21] Therefore, it is highly desirable but challenging to synthesize novel TiO_2 nanostructures as high-rate anode materials through a facile and green route. As an important group of solvents, ionic liquids (ILs), which exhibit unique properties including low volatility, a wide liquid temperature range, good dissolving ability, and designability, have been intensively used in organic synthesis, catalysis, and inorganic nanomaterials synthesis.[23–26] This inspires us to design a facile ILs-based synthetic system to prepare an attractive framework for high-efficiency lithium storage.

One such framework of TiO_2 active materials is ultrathin 2D nanosheets, which allow ultrafast surface lithium storage due to maximized Li^+ ion diffusion and electron transport and the elimination of the Li^+ ion diffusion process in TiO_2 bulk. However, it is not practical to obtain such a structure directly because of the Ostwald ripening process. IL-based systems may provide one possible way to obtain such desired materials. But there are still some technical issues to overcome, which include: 1) choice of an appropriate IL system from numerous candidates; 2) improvement of the thermal stability and avoidance of deformation or condensation of the obtained materials; and 3) retention of highly active surfaces or open channels. Herein, we report a facile and green route for large-scale synthesis of carbon-supported stacked TiO_2 nanosheets (CTNSs) using a simple and clean IL system. The carbon pillars in these CTNSs provide open channels for ultrafast lithium ion diffusion and the ultrathin framework renders the storage of lithium almost exclusively on the surface. As a result, the designed materials exhibit superior capacity and high-rate performance (191 mA h g^{-1} and 109 mA h g^{-1} at rates of 2 C and 50 C, respectively).

We approached the fabrication of titanate nanosheets as thin as single-unit-cell thickness by designing a special protic IL system in the presence of Li^+ ions. The protic IL, $[(CH_3)_2N^+(H)C_2H_4OH][CH_3COO^-]$, was obtained by directly mixing acetic acid and *N*,*N*-dimethylethanolamine. In this system, the IL is an excellent solvent with high density and low vapor pressure. In addition, the IL could act as an effective structure-directing agent for a layered framework and the –OH groups can easily connect to O and N to form intermolecular hydrogen bonds. With the aid of these abundant hydrogen bonds, the well-organized organic molecular layers could be formed with good stability. Tetrabutyl titanate ($Ti(OC_4H_9)_4$) serves as the titanium source. Moreover, the direction of crystal growth is regulated by Li^+ ions in this system.

The formation mechanism of the CTNSs is proposed and schematically illustrated in **Figure 1**. With the aid of Li^+ ions and strong hydrogen bonds in the IL system, the stable dagwood-like structure is stacked in an orderly way with alternating ultrathin titanate nanosheets and IL molecular layers. When annealed at 350 °C, the CTNS sample could be formed as a

J. H. Liu, X. F. Wei, Prof. X.-W. Liu
School of Physical & Mathematical Sciences
Nanyang Technological University
Singapore 637371, Singapore
E-mail: xuewei@ntu.edu.sg
J. S. Chen, Prof. X.-W. Lou
School of Chemical and Biomedical Engineering
Nanyang Technological University
Singapore 639798, Singapore
E-mail: xwlou@ntu.edu.sg

DOI: 10.1002/adma.201003759

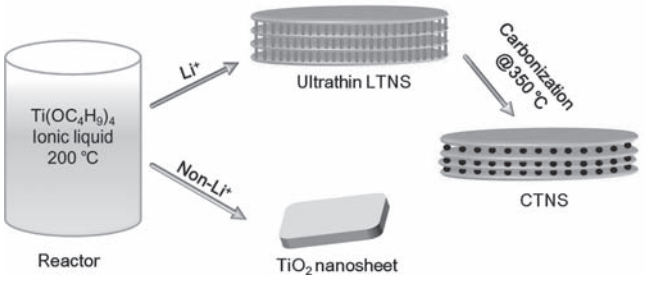

Figure 1. The proposed formation mechanism of CTNS with a sandwich-like multilamellar structure

result of the in situ carbonization of organic molecular layers. Interestingly, layered titanate nanosheets (LTNSs) could not be obtained in the absence of Li^+ ion under the same reaction condition. Li^+ ions may play a role as the other structure-directing agent in limiting the crystal growth along [010] direction and forming stable layered titanate nanosheets together with the IL. To the best of our knowledge, this is one of the first in its kind reporting thermally stable multilamellar nanostructures by stacking of ultrathin nanosheets.[27]

The morphologies of the samples were examined by transmission electron microscopy (TEM). From the TEM images, the as-synthesized sample consists of LTNSs with a lateral size of 20–50 nm (**Figure 2**a), and the magnified image displays the layered structure with an interlamellar spacing of ≈1 nm. The high-resolution (HR) TEM image (Figure 2b) of the gray sample obtained by annealing at 350 °C for 2 h, clearly shows that the disc-like nanostructures are formed by stacking of several ultrathin nanosheets. The single layer thickness of ≈0.4 nm is consistent with the single-unit-cell thickness along the [010] direction. Therefore, the nanosheets should be bound by (010) facets, which is also revealed by the 2D lattice fringes observed via HRTEM (Figure S1, Supporting Information). The exposed (010) facets are considered the ideal facet, possessing empty zigzag channels with large Ti–Ti distances for lithium ion diffusion.[22]

The layered structure of the as-synthesized sample was also observed by powder X-ray diffraction (XRD) analysis (Figure 2c). The strong Bragg peak at $2\theta = 8.48°$ from the as-synthesized LTNSs indicates a well-defined multilamellar structure with an interlayer spacing of 10.41 Å, which is consistent with the result from the TEM analysis. The peak intensity decreases significantly when the annealing temperature is increased from 250 to 300 °C, due to the carbonization of the intercalated organic components in the LTNSs. After calcination at 350 °C, the ordered LTNSs are superseded by the disordered ones. At the same time, the anatase TiO_2 phase becomes pronounced

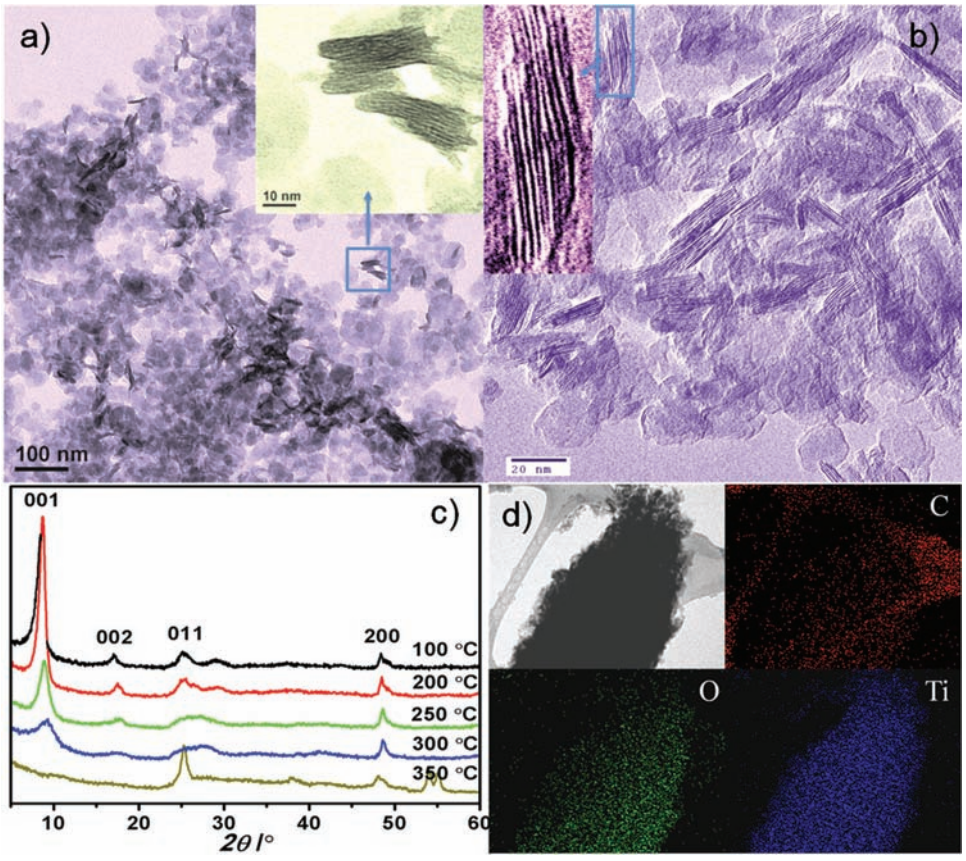

Figure 2. TEM images of the as-synthesized LTNSs (a) and the CTNSs obtained after annealing at 350 °C for 2 h (b). XRD patterns of the samples annealed at different temperatures (100, 200, 250, 300, and 350 °C) (c) and elemental mapping of CTNSs (d). The insets in (a) and (b) are the magnified images of the corresponding samples.

from the XRD pattern, indicating partial collapse of LTNS to form ultrathin anatase TiO_2 nanosheets. Further increasing the annealing temperature to 400 °C leads to complete removal of the nanocarbon components and formation of pure anatase TiO_2 phase (JCPDS no. 21 – 1272; Figure S2, Supporting Information).

The presence of C, O, and Ti was detected by elemental mapping and energy-dispersive X-ray (EDX) analysis of the sample as shown in Figure 2d. The uniformly dispersed carbon component in the CTNSs is derived by in situ carbonization of the residual organic species that stabilize the LTNSs. The corollary is also supported by thermogravimetric analysis (TGA; Figure S3, Supporting Information). The TGA curve of the LTNSs shows a total weight loss of ca. 25% which was recorded from room temperature to 500 °C, during which the organic components have been removed completely. Apparently, the sample annealed at 350 °C still contains about 5.6% nanocarbons by weight, compared with the sample annealed at 200 °C. These nanocarbon pillars not only strengthen the stacked ultrathin layers and prevent complete condensation, but also offer ample space for Li^+ ion diffusion.

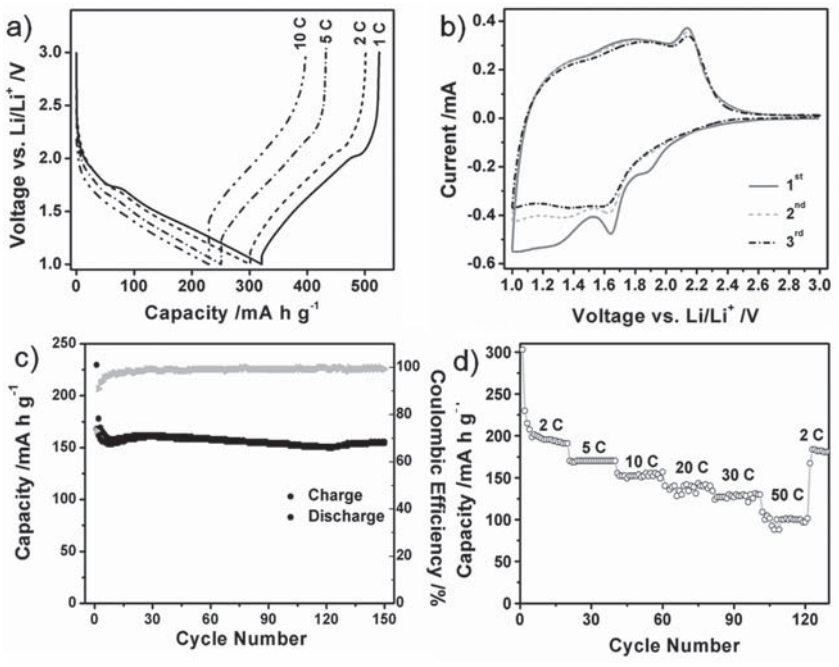

Figure 3. Electrochemical measurements of the CTNSs. a) The first-cycle charge–discharge voltage profiles at different current rates of 1 C, 2 C, 5 C, and 10 C. b) Representative cyclic voltammograms at a scan rate of 1 mV s^{-1}. c) Cycling performance of the CTNSs cycled at a constant current drain of 10 C and the corresponding Coulombic efficiency and d) cycling performance at different charge–discharge rates (2–50 C).

The samples were further characterized by N_2 adsorption–desorption isotherms and corresponding pore size distributions (Figure S4 and S5, Supporting Information). It is interesting to observe the abrupt increase of the pore fraction with size above ≈1 nm in the as-synthesized LTNSs. This observation might be related to the uniform stacked structure. The surface area and total pore volume of the CTNSs are 109 $m^2 g^{-1}$ and 0.09 $cm^3 g^{-1}$, respectively. Notably, the CTNSs possess smaller total pore volume but larger pore diameter compared with LTNSs because of the carbonization of organic components. In addition, Fourier transform infrared (FTIR) and Raman spectra further support our analysis of carbonization. The FTIR spectra (Figure S6, Supporting Information) shows the absorption bands of C–H and C–OH bonds in CTNSs sample are almost flattened. The crystallinity of the carbon in Raman spectra is indiscernible (Figure S7, Supporting Information). It may be due to the difficulty in forming highly crystalline carbon by carbonization of the single organic layer in intercalation at such a low temperature.

Solid-state ^{13}C and ^{1}H NMR spectra were employed to support the proposed mechanism. The organic carbon component in the intercalated IL layers can be identified using the cross polarization/magic angle spinning (CP/MAS) solid state ^{13}C NMR spectrum (Figure S8, Supporting Information). In general, it is anticipated that the removal of IL layers will lead to complete condensation of the layered titanate structure during the annealing processes at 350 °C. However, the CP/MAS solid state ^{1}H NMR spectrum (Figure S9, Supporting Information) shows that these organic components are partially carbonized at 350 °C in situ, due to the strong bonding force between the titanate and organic layers. This provides strong evidence for the formation of nanocarbons. Therefore, it can be concluded that the final structure is the CTNSs, based on the analyses mentioned above.

The electrochemical studies of the CTNSs obtained by annealing LTNSs at 350 °C were conducted using two-electrode Swagelok-type cells with lithium metal serving as both the counter and reference electrodes at room temperature.[18,28] The details are provided in the Experimental Section. The charge–discharge voltage profiles of the first cycle are shown in **Figure 3**a. The first cycle discharge capacities at different current drains of 1 C, 2 C, 5 C, and 10 C (1 C = 170 mA g^{-1}) are 321.2, 301.2, 250.6, and 229.6 mA h g^{-1}, respectively. The capacity of 321 mA h g^{-1} corresponds to $x = 0.96$ in Li_xTiO_2 for the first lithium insertion at a current drain of 1 C. Even more interestingly, each discharge–charge curve has an almost immutable gradient at different rates, and this behavior is completely different from that of the anatase TiO_2 materials annealed at 400 °C (Figure S10, Supporting Information), which shows the characteristic plateaus at specific voltages during charge–discharge.[18,29,30] The exact mechanism for this unusual behavior remains unclear at this moment. It is likely to be related to the unique structure of these CTNSs, in which the grain boundaries are improved by the strong interaction of the amorphous carbon with the TiO_2 crystalline and ultrathin 2D nanosheet structure.[4] More specifically, the Li^+ ion diffusion and charge transfer activity could take place mainly on the surface of these CTNSs, which mimic the features in electrochemical capacitors. As a result, the intrinsic voltage plateaus related to biphasic transformation are not observed.[31] Carbon

nanomaterials and ultrafine TiO_2 nanocrystals also exhibit the similar loss of voltage plateaus, owing to their highly efficient grain boundaries that stem from their porous structure and reduced size.[28,32,33]

The cyclic voltammetric curves (Figure 3b) are also different from those of other anatase TiO_2-based anodes. It shows that the broad peaks are present during the cathodic and anodic sweep. This could be attributed to the unique structure of the CTNSs, which is similar to that of the graphitic carbon with open channels for Li insertion and extraction reported.[34] Nevertheless, the signature current peaks of TiO_2 are still visible at voltages of ≈1.65 V and ≈2.1 V.

Figure 3c shows the cycling performance of the CTNSs at a current drain of 10 C. The discharge capacity loss in the initial cycles stems from the irreversible replacement of the protons on CTNSs surface by lithium ion when discharging the battery.[35] After 150 charge–discharge cycles a reversible discharge capacity as high as 155 mA h g^{-1} can still be retained, and the coulombic efficiency (calculated from the discharge and charge capacities) approaches almost 100%. The rate performance of the CTNSs at 2–50 C was further investigated as shown in Figure 3d, which clearly demonstrates excellent cyclability at all current rates. At lower rates, the discharge capacities at 2 C and 5 C are around 191 mA h g^{-1} and 170 mA h g^{-1}, respectively. It can still retain 135 and 125 mA h g^{-1} at 20 C and 30 C, respectively. Even at the highest rate of 50 C (8.5 A g^{-1}), a capacity of 109 mA h g^{-1} can be delivered. Evidently, the electrochemical performance of our CTNSs is superior to that of most previously reported TiO_2-based nanomaterials obtained under similar testing conditions.[18] The electrochemical studies demonstrate that the CTNSs exhibit a superior reversible capacity, excellent cycling performance, and good rate capability. The stable structure is further confirmed by the post-mortem XRD results (Figure S11, Supporting Information).

Comparative experiments were conducted to investigate the effect of calcination temperature and lithium ion concentration. The samples obtained by annealing LTNSs at 200 and 400 °C give lower capacities compared to the one annealed at 350 °C. After 100 full charge–discharge cycles, their discharge capacities remain only 91 and 125 mA h g^{-1} at a current drain of 5 C respectively (Figure S12, Supporting Information). TiO_2 nanosheets are obtained at 200 °C in the absence of Li^+ ion in the synthesis system as shown in **Figure 4**a. However, these nanosheets annealed at 350 °C exhibit a much lower capacity of no more than 100 mA h g^{-1} at 5 C after the same annealing treatment (Figure 4b). The synergetic effect of the IL and lithium ions, as well as the reaction temperature, could play an important role in the formation of stable LTNSs.

In summary, sandwich-like CTNSs are synthsized on a large scale by a facile and clean route. Owing to the unique textural features, i.e., stacked nanosheets with open channels, the storage of lithium in these CTNSs mainly takes place on surface, which is completely different from the insertion of lithium into bulk anatase TiO_2 materials. This pseudocapacitive insertion and extraction renders remarkable improvement in high-rate charging and discharging. Moreover, the in situ derived carbon can significantly stabilize these stacked TiO_2 nanosheets, leading to an excellent cycle life. We thus anticipate the promising use of this material in high-power lithium-ion batteries.

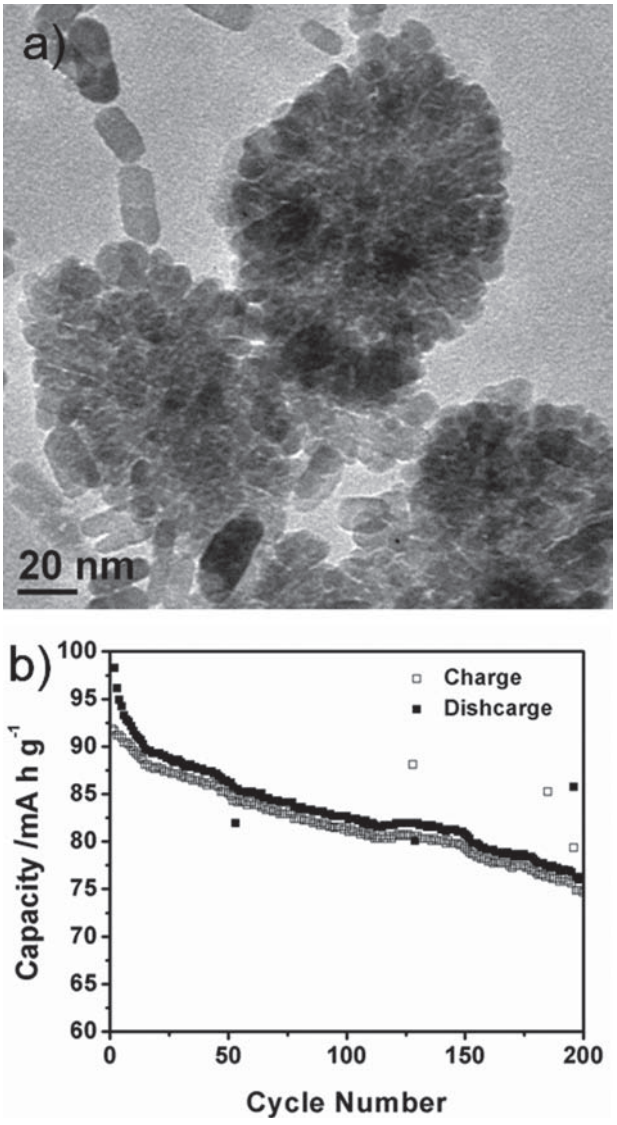

Figure 4. a) TiO_2 nanosheets obtained in the IL solution without Li^+ ion; b) Charge–discharge curves of the TiO_2 nanosheets annealed at 350 °C cycled at a constant current drain of 5 C.

Experimental Section

Synthesis of Ionic Liquid: The synthesis of IL was carried out in a 500-mL round-bottomed flask, which was immersed in an ice-bath. Acetic acid (60.0 g, 1.0 mol) was added dropwise into the *N*,*N*-dimethylethanolamine (98 g, 1.1 mol). After vigorous stirring for 2 h, the obtained protic IL was directly used to prepare the titanate material.

Preparation of Samples: In a typical experiment, 11 g of tetrabutyl titanate was first added to 50 g of IL containing CH_3COOLi (0, 0.01, or 0.04 mol) to form the tetrabutyl titanate–IL solution. The solution was transferred into teflon-lined stainless steel reactors and then heated at 200 °C for 10 h. After reaction, a white powder was obtained by centrifugation, washed with ethanol and water several times, and then dried in oven at 100 °C for 10 h. The annealing time of each sample was 2 h at different temperatures (200, 250, 300, 350, and 400 °C).

Characterization: XRD measurement was performed with a D8 diffractometer with Cu-KR radiation (λ = 1.54056 Å). TEM examination was carried out with JEOL JEM-1400 and JEOL 2100F. N_2 adsorption–desorption isotherms were conducted at 77 K on a Micromeritics Tristar 3000 analyzer. The BET surface areas and pore-size distribution curves were calculated using adsorption data. Thermogravimetric analysis was determined using a thermal gravity analyzer (TGA) at a temperature rise rate of 10 °C min^{-1} from room temperature to 600 °C under a continuous air flow. For ^{13}C and ^{1}H CP/MAS or magic angle spinning (MAS) NMR measurements, a JNM-ECA400 spectrometer was used at 100.5 and 400.0 MHz, respectively. FTIR spectra were recorded on a Shimazu IR Prestige-21 FT-IR Spectrometer. Raman spectra were collected on an R-3000HR spectrometer using a red LED laser (λ = 785 nm).

Electrochemical Measurements: The electrochemical tests were performed using two-electrode Swagelok-type cells with lithium serving as both the counter and reference electrodes at room temperature. The working electrode was composed of 70 wt% of the active material, 20 wt% of conductivity agent (carbon black, Super-P-Li), and 10 wt% of binder (polyvinylidene difluoride (PVDF), Aldrich). The active material (CTNS) was about 1–2 mg on each electrode and the film was about 20 μm in thickness. The electrolyte used was 1 M $LiPF_6$ in a 1:1 (w/w) mixture of ethylene carbonate and diethyl carbonate. Cell assembly was carried out in an argon-filled glove box. Cyclic voltammetry (CV; 1–3 V, 1 mV s^{-1}) was performed using an electrochemical workstation (CHI 660C). Galvanostatic charge–discharge cycling was conducted using a battery tester (NEWAER) with a voltage window of 1–3 V at different current rates of 1 C, 2 C, 5 C, 10 C, 20 C, 30 C, and 50 C, where 1 C = 170 mA g^{-1}.

Supporting Information

Supporting Information is available from the Wiley Online Library or from the author.

Acknowledgements

The authors acknowledge financial support from Nanyang Technological University (RG54/07) and the Ministry of Education (ARC24/07, T206B1218RS; AcRF Tier-1, RG63/08, M52120096), Singapore.

Received: October 12, 2010
Revised: November 19, 2010
Published online: December 27, 2010

[1] A. S. Arico, P. Bruce, B. Scrosati, J. M. Tarascon, W. Van Schalkwijk, *Nat. Mater.* **2005**, *4*, 366.
[2] A. Yamada, H. Koizumi, S. I. Nishimura, N. Sonoyama, R. Kanno, M. Yonemura, T. Nakamura, Y. Kobayashi, *Nat. Mater.* **2006**, *5*, 357.
[3] a) M. Gratzel, *Acc. Chem. Res.* **2009**, *42*, 1788; b) P. Simon, Y. Gogotsi, *Nat. Mater.* **2008**, *7*, 845.
[4] P. G. Bruce, B. Scrosati, J. M. Tarascon, *Angew. Chem. Int. Ed.* **2008**, *47*, 2930.
[5] J. B. Goodenough, Y. Kim, *Chem. Mater.* **2010**, *22*, 587.
[6] D. Deng, M. G. Kim, J. Y. Lee, J. Cho, *Energy Environ. Sci.* **2009**, *2*, 818.
[7] M. S. Whittingham, *Chem. Rev.* **2004**, *104*, 4271.
[8] A. R. Armstrong, G. Armstrong, J. Canales, R. García, P. G. Bruce, *Adv. Mater.* **2005**, *17*, 862.
[9] Y.-S. Hu, L. Kienle, Y.-G. Guo, J. Maier, *Adv. Mater.* **2006**, *18*, 1421.
[10] M. Wagemaker, W. J. H. Borghols, F. M. Mulder, *J. Am. Chem. Soc.* **2007**, *129*, 4323.
[11] X. Chen, S. S. Mao, *Chem. Rev.* **2007**, *107*, 2891.
[12] M. Wagemaker, F. M. Mulder, A. Van Der Ven, *Adv. Mater.* **2009**, *21*, 2703.
[13] N. A. Milne, M. Skyllas-Kazacos, V. Luca, *J. Phys. Chem. C* **2009**, *113*, 12983.
[14] W. B. Yue, C. Randorn, P. S. Attidekou, Z. X. Su, J. T. S. Irvine, W. Z. Zhou, *Adv. Funct. Mater.* **2009**, *19*, 2826.
[15] Y. G. Guo, Y. S. Hu, W. Sigle, J. Maier, *Adv. Mater.* **2007**, *19*, 2087.
[16] D. H. Kim, J. S. Jang, S. S. Han, K. S. Lee, S. H. Choi, A. Umar, J. W. Lee, D. W. Shin, S. T. Myung, J. S. Lee, S. J. Kim, Y. K. Sun, *J. Phys. Chem. C* **2009**, *113*, 14034.
[17] S. K. Das, A. J. Bhattacharyya, *J. Phys. Chem. C* **2009**, *113*, 17367.
[18] J. S. Chen, X. W. Lou, *Electrochem. Commun.* **2009**, *11*, 2332.
[19] X. G. Han, Q. Kuang, M. S. Jin, Z. X. Xie, L. S. Zheng, *J. Am. Chem. Soc.* **2009**, *131*, 3152.
[20] H. G. Yang, C. H. Sun, S. Z. Qiao, J. Zou, G. Liu, S. C. Smith, H. M. Cheng, G. Q. Lu, *Nature* **2008**, *453*, 638.
[21] J. S. Chen, Y. L. Tan, C. M. Li, Y. L. Cheah, D. Y. Luan, S. Madhavi, F. Y. C. Boey, L. A. Archer, X. W. Lou, *J. Am. Chem. Soc.* **2010**, *132*, 6124.
[22] G. Nuspl, K. Yoshizawa, T. Yamabe, *J. Mater. Chem.* **1997**, *7*, 2529.
[23] M. Antonietti, D. B. Kuang, B. Smarsly, Z. Yong, *Angew. Chem. Int. Ed.* **2004**, *43*, 4988.
[24] a) F. Endres, *ChemPhysChem* **2002**, *3*, 144; b) N. Kristian, Y. Yu, P. Gunawan, R. Xu, W.-Q. Deng, X.-W. Liu, X. Wang, *Electrochim. Acta* **2009**, *54*, 4916.
[25] T. L. Greaves, C. J. Drummond, *Chem. Soc. Rev.* **2008**, *37*, 1709.
[26] Z. G. Li, Z. Jia, Y. X. Luan, T. C. Mu, Opi. *Solid State Mater. Sci.* **2009**, *12*, 1.
[27] M. Choi, K. Na, J. Kim, Y. Sakamoto, O. Terasaki, R. Ryoo, *Nature* **2009**, *461*, 246.
[28] J. S. Chen, X. W. Lou, *J. Power Sources* **2010**, *195*, 2905; b) Y. Wang, W.-Q. Deng, X.-W. Liu, X. Wang, *Int. J. Hydrogen Energy* **2009**, *34*, 1437; c) Y. Yu, Y. Hu, X.-W. Liu, W.-Q. Deng, X. Wang, *Electrochim. Acta* **2009**, *54*, 3092.
[29] K. Kang, Y. S. Meng, J. Breger, C. P. Grey, G. Ceder, *Science* **2006**, *311*, 977.
[30] B. Kang, G. Ceder, *Nature* **2009**, *458*, 190.
[31] M. Wagemaker, A. P. M. Kentgens, F. M. Mulder, *Nature* **2002**, *418*, 397.
[32] N. A. Kaskhedikar, J. Maier, *Adv. Mater.* **2009**, *21*, 2664.
[33] J. Chen, J. Z. Wang, A. I. Minett, Y. Liu, C. Lynam, H. K. Liu, G. G. Wallace, *Energy Environ. Sci. Int. Ed.* **2009**, *2*, 393.
[34] D.-W. Wang, F. Li, M. Liu, Gao Q. Lu, H.-M. Cheng, *Angew. Chem.* **2008**, *47*, 373.
[35] W. J. H. Borghols, D. Lutzenkirchen-Hecht, U. Haake, W. Chan, U. Lafont, E. M. Kelder, E. R. H. van Eck, A. P. M. Kentgens, F. M. Mulder, M. Wagemaker, *J. Electrochem. Soc.* **2010**, *157*, A582.